

# Morse index and bifurcation for figure-eight choreographies of the equal mass three-body problem

Hiroshi Fukuda<sup>1</sup>, Toshiaki Fujiwara<sup>1</sup> and Hiroshi Ozaki<sup>2</sup>

<sup>1</sup> College of Liberal Arts and Sciences, Kitasato University, 1-15-1 Kitasato, Sagami-hara, Kanagawa 252-0329, Japan

<sup>2</sup> Laboratory of general education for science and technology, Faculty of Science, Tokai University, 4-1-1 Kita-Kaname, Hiratsuka, Kanagawa, 259-1292, Japan

E-mail: fukuda@kitasato-u.ac.jp, fujiwara@kitasato-u.ac.jp and ozaki@tokai-u.jp

2 January 2022

**Abstract.** We report on the Morse index and periodic solutions bifurcating from the figure-eight choreography for the equal mass three-body problem under homogeneous potential  $-1/r^a$  for  $a \geq 0$ , and under Lennard-Jones (LJ) type potential  $1/r^{12} - 1/r^6$ , where  $r$  is a distance between bodies. It is shown that the Morse index changes at a bifurcation point and all solutions bifurcating are approximated by variational functions responsible for the change of the Morse index. Inversely we observed bifurcation occurs at every point where the Morse index changes for the figure-eight choreography under  $-1/r^a$ , and for  $\alpha$  solution under LJ type potential, where  $\alpha$  solution is a figure-eight choreography tending to that under  $-1/r^6$  for infinitely large period. Thus, to our numerical studies, change of the Morse index is not only necessary but also sufficient condition for bifurcation for these choreographies. Further we observed that the change of the Morse index is equal to the number of bifurcated solutions regarding solutions with congruent orbits as the same solution.

Submitted to: *J. Phys. A: Math. Theor.*

## 1. Introduction

Choreographic motion of  $n$  bodies is a periodic motion on a closed orbit,  $n$  identical bodies chase each other on the orbit with equal time-spacing. Moore [1] found a remarkable figure-eight choreographic solution for  $n = 3$  under homogeneous potential  $-1/r^a$  by numerical calculations, where  $r$  is a distance between bodies. Chenciner and Montgomery [2] gave a mathematical proof of its existence for  $a = 1$  by variational method. The detailed initial conditions for three bodies are found in [2, 3].

Sbano [4], and Sbano and Southall [5], studied  $n$ -body choreographic solutions under an inhomogeneous potential

$$u^{LJ}(r) = \frac{1}{r^{12}} - \frac{1}{r^6}, \quad (1)$$

a model potential between atoms called Lennard-Jones-type (hereafter LJ) potential. Sbano and Southall [5] proved that there exist at least two  $n$ -body choreographic solutions for sufficiently large period, and there exists no solution for small period. We confirmed their theorem numerically for  $n = 3$  and unexpectedly found a multitude of three-body figure-eight choreographic solutions under LJ-type potential (1) [6].

Following Shibayama's preliminary calculation for  $a = 1$  [7], we did accurate numerical calculation of the Morse index, for the three-body figure-eight choreography in the domain of periodic function [8]. Here the Morse index is a number of independent variational functions giving negative second variation of action functional.

In our paper [8], a strong relationship between the Morse index and H solution found by Simó [3], which is a periodic solution close to the figure-eight choreography but made up of three distinct orbits, was suggested. On the other hand Galán *et al* [9] showed that the H solution bifurcated from figure-eight choreography by changing the masses of three bodies. They also found many different periodic orbits on figure-eight [10].

There are several researches on the Morse index for periodic solution of three-body problem. Barutello *et al* [11] calculated the Morse index mathematically for the Lagrangian circular solution, and Hu and Sun [12, 13] for elliptic Lagrangian solutions, to discuss the linear stability.

In this paper, we show a relationship between the Morse index of the figure-eight choreographies and periodic solutions bifurcating for a system of three identical bodies interacting through a homogeneous potential or through LJ-type potential (1). In section 2, we show the Morse index changes at a bifurcation point and solutions bifurcating are approximated by variational functions responsible for change of the Morse index.

In section 3, we discuss the bifurcation from the figure-eight choreography under homogeneous potential,  $-1/r^a$ , by changing  $a$ . In section 3.1, we show the H solution bifurcates at  $a = 0.9966$  where the Morse index changes. In section 3.2, another bifurcation at  $a = 1.3424$  is shown. These bifurcations at  $a = 0.9966$  and  $1.3424$  are first found in 2005 by Muñoz-Almaraz *et al* [14, 15] using AUTO [16, 17]. There is no other point where the Morse index changes for  $a \geq 0$ .

In section 4, we discuss the bifurcation of the  $\alpha$  solution for the system under LJ-type potential, where the  $\alpha$  solution is a figure-eight choreography tending to that under  $-1/r^6$  for infinitely large period. There are seven points where the Morse index changes for the  $\alpha$  solution. In section 4.1 we show four points bifurcate periodic but non choreographic solutions, which are the same type of the bifurcations discussed in section 3. In section 4.2, we show the rest three points yield choreographic solutions less symmetric than figure-eight. Alain Chenciner, in ICM 2002, asked a question about

the existence of less symmetric figure-eight [18, 19]. We can say “Yes”, they exist under LJ-type potential. Section 5 is a summary and discussions.

Our numerical results in this paper were calculated by Mathematica 11.1.

## 2. Morse index and bifurcation

### 2.1. Morse index and eigenvalue problem

For a system of three identical bodies in classical mechanics, we consider periodic solutions to equations of motion,

$$\frac{d}{dt} \frac{\partial L}{\partial \dot{q}_i} = \frac{\partial L}{\partial q_i}, \quad i = 1, 2, \dots, 6, \quad (2)$$

where dot represents a differentiation in  $t$ .  $L$  is the Lagrangian with the potential energy  $U(q)$ ,

$$L = \sum_{i=1}^6 \frac{\dot{q}_i^2}{2} - U(q), \quad (3)$$

and

$$q(t) = (q_1(t), q_2(t), \dots, q_6(t))^* \quad (4)$$

a six component vector composed of position vectors

$$\mathbf{r}_b(t) = (x_b(t), y_b(t))^* = (q_{2b-1}(t), q_{2b}(t))^* \quad (5)$$

for body  $b = 1, 2, 3$  in a plane, where  $*$  represents transpose. The subscript of six component vector is assumed to be in the range between 1 and 6.

For a periodic solution  $q(t+T) = q(t)$  and variation function  $\delta q(t+T) = \delta q(t)$  with period  $T$ , the Morse index  $N$  is defined as a number of independent variation function  $\delta q(t)$  which make the second variation  $S^{(2)}$  with

$$S^{(k)} = \int_0^T dt \left( \sum_i (\delta q_i \frac{\partial}{\partial q_i} + \dot{\delta q}_i \frac{\partial}{\partial \dot{q}_i}) \right)^k L \quad (6)$$

of the action functional

$$S(q) = \int_0^T L(q, \dot{q}) dt \quad (7)$$

negative. Since the  $S^{(2)}$  is written as

$$S^{(2)} = (\delta q, \hat{H} \delta q) \quad (8)$$

by  $6 \times 6$  matrix operator  $\hat{H}$ ,

$$(\hat{H})_{ij} = -\delta_{ij} \frac{d^2}{dt^2} - \frac{\partial^2 U}{\partial q_i \partial q_j}, \quad (9)$$

the Morse index is a number of negative eigenvalues of the eigenvalue problem,

$$\hat{H}\psi = \lambda\psi, \quad (10)$$

$$\psi(t + T) = \psi(t), \quad (11)$$

$$(\psi, \psi) = 1, \quad (12)$$

with the second variation

$$S^{(2)} = \lambda \quad (13)$$

and the variation function

$$\delta q = \psi, \quad (14)$$

where  $(f, g)$  is the inner product defined by

$$(f, g) = \int_0^T dt f^* g \quad (15)$$

and  $\delta_{ij}$  the Kronecker delta.

## 2.2. Bifurcation and eigenvalue problem

For a periodic solution of equation of motion (2) with some parameter  $\xi$ ,  $q(t; \xi)$ , suppose the other periodic solution  $q^b(t; \xi)$  bifurcates at  $\xi = \xi_0$ , that is,

$$\lim_{\xi \rightarrow \xi_0} q^b(t; \xi) = q(t; \xi_0). \quad (16)$$

Since for the Lagrangian (3)

$$\ddot{q} = -\frac{\partial U}{\partial q_i} \quad (17)$$

and

$$\ddot{q}^b = -\frac{\partial U}{\partial q_i^b}, \quad (18)$$

$\Delta q = q^b - q$  satisfies

$$\frac{d^2}{dt^2} \Delta q_i = -\left. \frac{\partial U}{\partial q_i} \right|_{q=q^b} + \frac{\partial U}{\partial q_i} = -\sum_j \frac{\partial^2 U}{\partial q_j \partial q_i} \Delta q_j + O(|\Delta q|^2), \quad (19)$$

that is,

$$\hat{H} \Delta q \rightarrow 0 \text{ for } \xi \rightarrow \xi_0. \quad (20)$$

Thus equation (20) is a necessary condition for  $\xi_0$  to be a bifurcation point.

When  $\xi \rightarrow \xi_0$ , equation (20) shows that  $\Delta q$  goes to the eigenfunction of  $\hat{H}$  whose eigenvalue  $\lambda$  is zero. In other words, at a bifurcation point some eigenvalue  $\lambda$  of  $\hat{H}$  has to go to zero. Thus, using the normalized eigenfunctions  $\psi^{(k)}$  of the eigenvalue  $\lambda \rightarrow 0$  we have an approximate expression by variated orbit

$$Q = q + h \sum_k^g c_k \psi^{(k)} \quad (21)$$

for the bifurcating solution

$$q^b = q + \Delta q \rightarrow Q \text{ for } \xi \rightarrow \xi_0, \quad (22)$$

where  $g$  is a degeneracy of the  $\lambda$ ,  $c_k$  and  $h$  are real coefficients with  $\sum_k^g c_k^2 = 1$  and  $h \rightarrow 0$ . Since the variated orbit  $Q$  has its own symmetry independent of  $\xi$  and  $h$  [8], bifurcating solution  $q^b$  will be found within the symmetry.

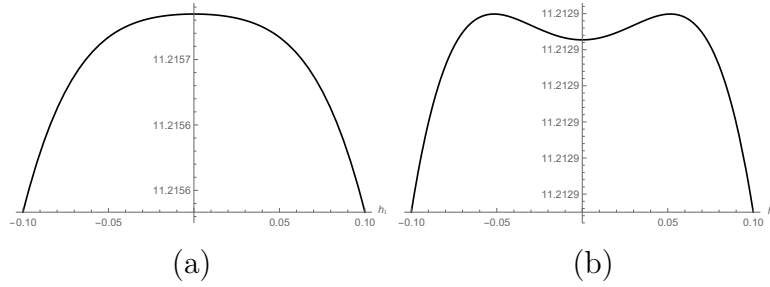


**Figure 1.** An action functional  $S(q + h_1 \psi^{(1)})$  for  $\Delta N = -1$ . Bifurcation is supposed to be one side in  $\xi > \xi_0$ . (a)  $\xi < \xi_0$ . (b)  $\xi > \xi_0$ .

### 2.3. Morse index and bifurcation

We define change of the Morse index  $N(\xi)$  by

$$\Delta N(\xi) = \lim_{\xi' \rightarrow \xi+0} N(\xi') - \lim_{\xi' \rightarrow \xi-0} N(\xi'). \quad (23)$$

Thus

$$g = |\Delta N(\xi_0)| \quad (24)$$

and an eigenvalue  $\lambda(\xi)$  changes the sign at  $\xi = \xi_0$ ,

$$\Delta N(\xi_0)(\xi - \xi_0)\lambda(\xi) \leq 0 \quad (25)$$

around  $\xi_0$ .

Then the sign of the action,

$$\Delta S(\xi) = S(q^b(t; \xi)) - S(q(t; \xi)), \quad (26)$$

has the same sign as  $\lambda(\xi)$

$$\Delta S(\xi)\lambda(\xi) \geq 0 \quad (27)$$

and

$$\Delta N(\xi_0)(\xi - \xi_0)\Delta S(\xi) \leq 0 \quad (28)$$

around  $\xi_0$ . Since  $S$  is expanded in  $h$  with coefficients (6) as

$$S(q + h\delta q) = S^{(0)} + hS^{(1)} + \frac{h^2}{2!}S^{(2)} + \dots, \quad (29)$$

and  $q^b$  tends to  $Q = q + h\delta q$  with  $\delta q = \sum_k^g c_k \psi^{(k)}$  for  $\xi \rightarrow \xi_0$ ,

$$\Delta S(\xi) \rightarrow S(Q) - S(q) = \frac{h^2}{2}S^{(2)} + \frac{h^3}{3!}S^{(3)} + \dots = \frac{h^2}{2}\lambda + O(h^3). \quad (30)$$

Thus (27) then (28) are derived by (30).

On the basis of  $\Delta N$ , (27) and (28), we can picture bifurcation through manifold of action functional  $S$  in the subspace of corresponding  $\lambda$ . For example, suppose  $\Delta N = -1$  and bifurcation is one side in  $\xi > \xi_0$ . Thus, in the one dimensional subspace of  $\lambda$ , top of a local maximum in  $S$  where  $q$  locates for  $\xi < \xi_0$ , shown in figure 1 (a), will slightly cave in for  $\xi > \xi_0$ , which yield critical points for  $q^b$  in the both sides of the cave, shown

**Table 1.**  $\Delta N(a)$  and symmetry of  $Q$  for  $a \geq 0$ .

$a$	$\Delta N(a)$	$Q$
0.9966	-2	$D_y$
1.3424	-2	$D$

in figure 1 (b). We confirmed that the inequalities (27) and (28) corresponding to the picture of bifurcation as shown in figure 1 hold in our numerical calculations.

We define an equivalent class, congruent class of bifurcated solutions  $B$ , by regarding the bifurcated solutions with congruent orbits as equivalent, and denote the number of elements by  $\#B$ . Then we define number of incongruent bifurcated solutions as

$$N_B = \lim_{\xi' \rightarrow \xi - 0} \#B(\xi') + \lim_{\xi' \rightarrow \xi + 0} \#B(\xi'). \quad (31)$$

In the following sections we will show

$$N_B = |\Delta N| \quad (32)$$

holds for  $\xi = \xi_0$  in our numerical calculations.

Note that at a bifurcation point the Morse index may not change,  $\Delta N = 0$ , if  $\lambda = 0$  but  $d\lambda(\xi)/d\xi = 0$ . However for figure-eight choreographies in this paper, such point never contribute to any bifurcation and belongs to  $\lambda = 0$  in the whole region of  $\xi$  corresponding to the conservation laws. In other words, (32) holds not only for  $\xi = \xi_0$  but also for all  $\xi$ .

We call the region  $\xi < \xi_0$  the left side of the bifurcation point  $\xi_0$  and  $\xi_0 < \xi$  the right side.

### 3. Morse index and bifurcation for homogeneous system

In this section we investigate the bifurcation of the figure-eight choreography by using  $a$  as the parameter  $\xi$  for a system under homogeneous potential

$$U(q) = \sum_{b>c} u_a(|(q_{2b-1} - q_{2c-1}, q_{2b} - q_{2c})|), \quad u_a(r) = -\frac{1}{r^a}, \quad (33)$$

for  $a \geq 0$ . In table 1,  $a$ ,  $\Delta N(a) \neq 0$  and symmetry of the variated orbit  $Q$  are tabulated. The symbol  $D$  means that the  $Q$  is not choreographic, and the subscript  $y$  indicates that the orbits are symmetric in the  $y$  axis. There is no other point with  $\Delta N(a) \neq 0$  for  $a \geq 0$  than tabulated in table 1,  $a = 0.9966$  and  $1.3424$ .

#### 3.1. Bifurcation at $a = 0.9966$

At  $a = 0.9966$ , the Morse index  $N(a)$  changes by  $\Delta N = -2$  as shown in table 1. For  $g = |\Delta N| = 2$ , the variated orbit  $Q$  is written as

$$Q = q + h(\cos \Theta \psi^{(1)} + \sin \Theta \psi^{(2)}) \quad (34)$$

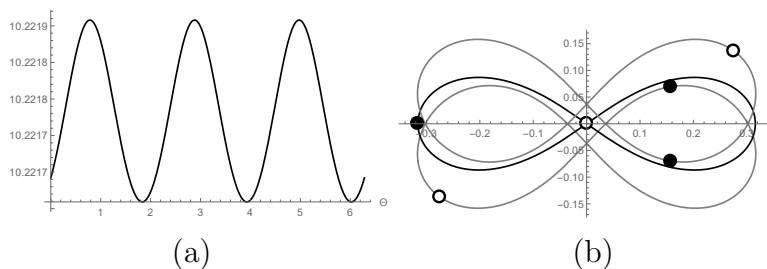


**Figure 2.** Variated orbit  $Q$  in (34) for  $a = 1$  close to  $a = 0.9966$ ;  $T = 1$ ,  $h = 0.08$ ,  $\lambda = 0.06881$ . (a)  $S(Q)$  of  $\Theta$ . (b)  $Q$  with  $D_{xy}$  symmetry for a local maximum at  $\Theta = 0.78343$  in  $S(Q)$ . Note that the value of  $\Theta$  does not have universal meaning since it depends on the choice of orthonormal basis,  $\psi^{(1)}$  and  $\psi^{(2)}$ . Filled circles are isosceles triangle configuration at  $t = 0$  and open circles Euler configuration at  $t = T/4$ .

with  $c_1 = \cos \Theta$  and  $c_2 = \sin \Theta$ . The coefficients are, thus, found as critical points in  $\Theta$  by

$$\frac{\partial S(Q)}{\partial \Theta} = 0. \quad (35)$$

As shown in figure 2 (a) at  $h = 0.08$ , there are six critical points in  $S(Q)$  of  $\Theta$ , three local maximums and three local minimums, which are independent of  $h$ . At all six critical points in  $\Theta$ , the variated orbits  $Q$ 's have the same symmetry higher than the  $D_y$  indicated in table 1. They consist of three distinct orbits symmetric in the  $y$  axis and in the  $x$  axis with exchange of two bodies; one orbit is symmetric itself but two collectively. Thus we denote orbits with this symmetry by  $D_{xy}$ . In figure 2 (b), the variated orbit  $Q$  at a local maximum is shown. Black orbit is symmetric itself but two gray orbits collectively. Consequently all bifurcating solutions from  $a = 0.9966$  will be searched within  $D_{xy}$  symmetry. Note that since it is numerically difficult to calculate the  $Q$  just at the bifurcation point  $a = 0.9966$  and its symmetry does not depend on  $a$ , in figure 2 calculation for  $a = 1$  is shown.

Conditions for  $q(t)$  to be  $D_{xy}$ , derived in Appendix A.1, are that  $q(t)$  takes an isosceles triangle configuration at  $t = 0$  shown by filled circles in figure 2 (b),

$$q(0) = (x, y, -2x, 0, x, -y), \quad (36)$$

$$\dot{q}(0) = (-\cos \theta, -\sin \theta, 0, 2 \sin \theta, \cos \theta, -\sin \theta)v, \quad (37)$$

with

$$\theta = \tan^{-1} \frac{y}{3x}, \quad (38)$$

by parameters  $(x, y, v)$ , and an Euler configuration at  $t = T/4$  shown by open circles in figure 2 (b),

$$(q_3, q_4, \dot{q}_1 \dot{q}_6 - \dot{q}_2 \dot{q}_5) = 0. \quad (39)$$

For given period  $T$ , the three conditions (39) determine the three parameters  $(x, y, v)$ .

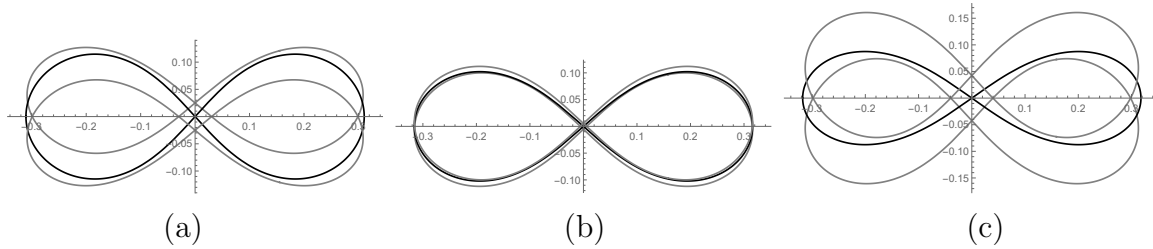


**Figure 3.**  $D_{xy}$  solutions bifurcated from  $a = 0.9966$ ; (a)  $a = 0.9766$ , (b)  $a = 1$ , and (c)  $a = 1.0166$ , for  $T = 1$ . Parameters  $(x, y, v; d)$  for (a)–(c) are  $(0.15533, 0.12092, 1.79372; 0.025027)$ ,  $(0.15800, 0.096588, 2.2321; -0.0054265)$  and  $(0.15886, 0.072493, 2.58066; -0.042498)$ , respectively.

In order to distinguish  $D_{xy}$  from figure-eight choreography which are very close around a bifurcation point, we use the  $y$  component of body 1 on the  $x$  axis,

$$d = q_2(t), \quad (40)$$

for  $t \simeq T/12$  with  $q_1(t) = 0$  since  $d$  is zero if and only if  $D_{xy}$  is choreographic.

Muñoz-Almaraz *et al* [14, 15] first found the bifurcation at  $a = 0.9966$  using AUTO [16, 17], and recently we re-found it using the equations (36)–(39) with Newton's method: three  $D_{xy}$  solutions corresponding to the three local maximums in  $S(Q)$  of  $\Theta$  bifurcate in the right side of the bifurcation point, and three to the local minimums in the left side.

The six critical points in figure 2 (a) are written by a position of local maximum  $\Theta_3$  as  $\Theta_3 + 2j\pi/3 + k\pi$ ,  $j = 0, 1, 2$ ,  $k = 0, 1$ . Thus the  $Q$  for the six solutions bifurcating in the both sides are represented by  $\Theta = \Theta_3 + 2j\pi/3$  with a smooth increasing function  $h$  of  $a$ . Using the choreographic operator  $\hat{C}$  defined by

$$\hat{C}f_i(t) = f_{i+2}(t - T/3) \quad (41)$$

since for the doubly degenerate eigenvalue [8, 20]

$$\hat{C}(\cos \Theta \psi^{(1)} + \sin \Theta \psi^{(2)}) = \cos(\Theta + 2\pi/3)\psi^{(1)} + \sin(\Theta + 2\pi/3)\psi^{(2)}, \quad (42)$$

the  $Q$  for  $D_{xy}$  is written as

$$Q^{D_{xy}} = q + h\hat{C}^j(\cos \Theta_3 \psi^{(1)} + \sin \Theta_3 \psi^{(2)}), \quad j = 0, 1, 2. \quad (43)$$

Since  $\hat{C}^3 = 1$  and  $\hat{C}q = q$ , representation (43) for  $j = 0, 1, 2$  differ only in cyclic permutation of bodies with time shift. Thus their orbits are congruent and the number of incongruent solutions  $N_B$  is counted as  $N_B = 1 + 1 = 2$ . In figure 3 (a) and (c), one of three congruent  $D_{xy}$  solutions in the both sides of bifurcation point,  $a = 0.9966 \pm 0.02$ , are shown with parameters  $(x, y, v)$  for initial condition and the index  $d$ .

As we showed in [8], the Simó's H solution is in good agreement with the variated orbit  $Q$  because it is the solution  $D_{xy}$  bifurcating from  $a = 0.9966$  very close to  $a = 1$ . Actually the solution  $D_{xy}$  at  $a = 1$  shown in figure 3 (b) coincides with the Simó's H solution.



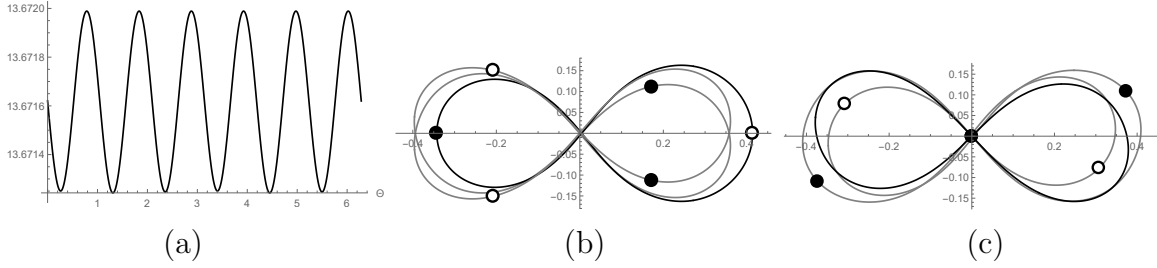


**Figure 4.** Variated orbit  $Q$  for  $a = 1.345$  close to  $a = 1.3424$ ;  $T = 1$ ,  $\lambda = 0.02095$ ,  $h = 0.1$ . (a)  $S(Q)$  of  $\Theta$ . (b)  $Q$  with  $D_x$  symmetry for a local maximum at  $\Theta = 0.78448$ . Note that the  $\Theta$  does not have universal meaning since it depends on the choice of orthonormal basis,  $\psi^{(1)}$  and  $\psi^{(2)}$ . Filled circles are isosceles triangle configuration at  $t = 0$  and open circles  $t = T/2$ . (c)  $Q$  with  $D_2$  for a local minimum at  $\Theta = 0.78448 + \pi/6$ . Filled circles are Euler configuration at  $t = 0$  and open circles at  $t = T/2$ .

### 3.2. Bifurcation at $a = 1.3424$

For  $a \geq 0$ , there is one more point changing the Morse index at  $a = 1.3424$  as shown in table 1. In this section we investigate this point in similar manner as in section 3.1.

The eigenvalue  $\lambda$  which goes to zero at  $a = 1.3424$  is doubly degenerate,  $g = |\Delta N| = 2$ , and the variated orbit  $Q$  in (34) are expected as bifurcating solutions. However its symmetry  $D$  shown in table 1 is lower than for  $D_y$  at  $a = 0.9966$ , and its action  $S(Q)$  as a function of  $\Theta$  exhibits twelve critical points; six local maximums and six local minimums as shown in figure 4 (a). In figure 4,  $S(Q)$  and  $Q$  for  $a = 1.345$  are shown as a close point to  $a = 1.3424$  because of numerical convenience.

At local maximums, the variated orbit  $Q$  consists of three distinct orbits: one orbit is symmetric itself in the  $x$  axis and the other two are collectively, shown in figure 4 (b). On the other hand, at local minimums: one orbit is symmetric itself at origin and the other two collectively, shown in figure 4 (c). We denote former by  $D_x$  and latter  $D_2$ . Here the orbits of  $D_x$  can have non zero total angular momentum  $l$  since sum of signed area of the three orbits can be non zero whereas it is zero for solutions  $D_2$ ,  $D_{xy}$  and the figure-eight choreography because of two fold symmetry at origin.

Conditions for  $q(t)$  to be  $D_x$ , derived in Appendix A.2, are that  $q(t)$  takes an isosceles triangle configuration shown by filled circles in figure 4 (b), (36) and (37) with

$$\theta = \tan^{-1} \frac{y}{3x} - \tan^{-1} \frac{l}{2v\sqrt{9x^2 + y^2}}, \quad (44)$$

at  $t = 0$  by parameters  $(x, y, v, l)$ , and opposite isosceles triangle configuration at  $t = T/2$  shown by open circles in figure 4 (b),

$$(q_4, \dot{q}_3, q_1 - q_5, \dot{q}_2 - \dot{q}_6) = 0. \quad (45)$$

For given period  $T$ , four conditions (45) determine four parameters  $(x, y, v, l)$ . An index to distinguish  $D_x$  from figure-eight choreography is

$$(d, l) \neq 0, \quad (46)$$

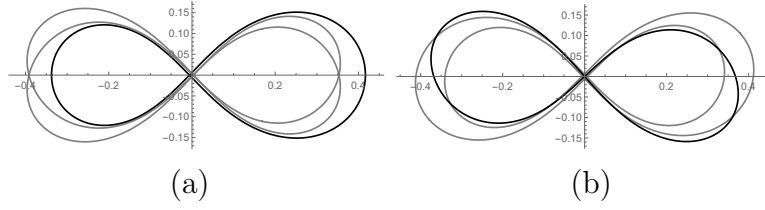


**Figure 5.** (a)  $D_x$  and (b)  $D_2$  solutions at  $a = 1.3425$  with  $T = 1$  bifurcated from  $a = 1.3424$ .  $D_2$  is rotated by  $\theta_2$  in (53). Parameters: (a)  $(x, y, v, l) = (0.16872, 0.11111, 2.8874, 0.000035433)$ , (b)  $(x, u, v; \Delta I) = (0.39375, 0.57707, 1.1697; -0.11584)$ .

since  $D_x$  with  $l = 0$  is the  $D_{xy}$  solution.

Conditions for  $q(t)$  to be  $D_2$ , derived in Appendix A.4, are that  $q(t)$  takes an Euler configuration at  $t = 0$  shown by filled circles in figure 4 (c),

$$q(0) = (x, 0, -x, 0, 0, 0), \quad (47)$$

$$\dot{q}(0) = (u, v, u, v, -2u, -2v) \quad (48)$$

by parameters  $(x, u, v)$ , and another Euler configuration at  $t = T/2$  shown by open circles in figure 4 (c),

$$(q_5, q_6, \dot{q}_1 \dot{q}_4 - \dot{q}_2 \dot{q}_3) = 0. \quad (49)$$

For given period  $T$ , three conditions (45) determine three parameters  $(x, u, v)$ . An index to distinguish  $D_2$  from figure-eight choreography is

$$(d, \Delta I) \neq 0, \quad (50)$$

where  $\Delta I = I(T/2) - I(0)$  and  $I(t) = |q(t)|^2 = \sum_i |q_i(t)|^2$ , since  $D_2$  with  $\Delta I = 0$  is the  $D_{xy}$  solution.

Using AUTO [16, 17], Muñoz-Almaraz *et al* found the solution  $D_x$  bifurcated at  $a = 1.3424$  in 2005 together with  $D_{xy}$  at  $a = 0.9966$  [14, 15]. Knowing the existence of  $D_x$ , we recently re-found  $D_x$  and  $D_2$  using the above equations with Newton's method: six  $D_x$  and six  $D_2$  solutions bifurcate in the right side of bifurcation point.

The six  $D_x$  solutions are written by the  $Q$  with  $\Theta$  at local maximums, and the six  $D_2$  at local minimums. The  $\Theta$ 's at local maximums are written by a position of local maximum  $\Theta_6$  as  $\Theta_6 + 2j\pi/6$  with integer  $j$ , and local minimums as  $\Theta_6 + (2j + 1)\pi/6$ . Thus, by (42), the  $Q$  for  $D_x$  and  $D_2$  solutions are represented by

$$Q^{D_x} = q \pm h \hat{C}^j (\cos \Theta_6 \psi^{(1)} + \sin \Theta_6 \psi^{(2)}), \quad (51)$$

and

$$Q^{D_2} = q \pm h \hat{C}^j (\cos(\Theta_6 + \pi/6) \psi^{(1)} + \sin(\Theta_6 + \pi/6) \psi^{(2)}), \quad (52)$$

respectively, with  $j = 0, 1, 2$  and  $a > 1.3424$ . In (51) and (52), the sign in front of  $h$  effects inversion of orbits in the  $y$  axis. Then the orbits of six  $D_x$  solutions are all congruent, in direct isometry or mirror inversion, and the orbits of six  $D_2$  solutions are so. Thus the number of incongruent bifurcating solutions  $N_B$  is counted as  $N_B = 0 + 2 = 2$ .

**Table 2.**  $\Delta N(T)$  and symmetry of  $Q$  for LJ  $\alpha_{\pm}$ . Symbols,  $C_x$ ,  $C_y$ ,  $C_{xy}$  and  $C_2$  mean that the  $Q$  is symmetric in the  $x$  axis, in the  $y$  axis, in both the  $x$  and the  $y$  axes and at origin, respectively.

$\alpha_-$			$\alpha_+$		
$T$	$\Delta N(T)$	$Q$	$T$	$\Delta N(T)$	$Q$
14.479		$C_{xy}$	16.111	2	$D$
14.595	-1	$C_x$	16.878	2	$D_y$
14.836	-2	$D_y$	17.132	1	$C_y$
14.861	-2	$D$	18.615	1	$C_2$

In figure 5, one of six congruent  $D_x$  and  $D_2$  solutions at  $a = 1.3425$  are shown with parameters for initial conditions and with  $\Delta I$  for  $D_2$ , where  $D_2$  is rotated by

$$\theta_2 = -\frac{1}{2} \tan^{-1} \frac{q_4(T/2)}{q_3(T/2)}, \quad (53)$$

to make the  $x$  axis bisector of two Euler configurations.

#### 4. Morse index and bifurcation for LJ system

In this section, we discuss the bifurcation of the  $\alpha$  solution by using  $T$  as the parameter  $\xi$  for the system under LJ-type potential

$$U(q) = \sum_{b>c} u^{LJ} (|(q_{2b-1} - q_{2c-1}, q_{2b} - q_{2c})|). \quad (54)$$

The  $\alpha$  solution bifurcates at  $T = T_{\min} = 14.479$ , thus there exists no  $\alpha$  solution for  $T < T_{\min}$  and two  $\alpha$  solutions for  $T > T_{\min}$ . One branch  $\alpha_-$  from  $T = T_{\min}$  of  $\alpha$  solution tends to the figure-eight choreography under homogeneous potential with  $a = 6$  for  $T \rightarrow \infty$ , and the other branch  $\alpha_+$  gourd-shaped for  $T \rightarrow \infty$  [8].

In table 2,  $T$ ,  $\Delta N(T) \neq 0$  and symmetry of the variated orbit  $Q$  for  $\alpha_+$  and  $\alpha_-$  are tabulated. Symbols,  $C_x$ ,  $C_y$ ,  $C_{xy}$  and  $C_2$  mean that the variated orbit  $Q$  is choreographic and is symmetric in the  $x$  axis, in the  $y$  axis, in both the  $x$  and the  $y$  axes, and at origin, respectively. Note that though the symbols  $C_x$  and  $C_{xy}$  were written as  $C$  and  $C_e$  in [8], respectively, we redefined them since  $C$  and  $C_e$  have the same symmetry as  $D_x$  and  $D_{xy}$ , defined in section 3.2, respectively. There is no other point with  $\Delta N(T) \neq 0$  for  $\alpha$  solution than seven points tabulated in table 2.

##### 4.1. Bifurcation yielding $D_{xy}$ , $D_x$ and $D_2$ solutions

The points indicated by  $D_y$  in table 2,  $T = 16.878$  for  $\alpha_+$  and  $T = 14.836$  for  $\alpha_-$ , yield  $D_{xy}$  solutions represented by (43) as in the section 3.1. The bifurcations are the both sides and the number of incongruent bifurcating solutions  $N_B$ 's are both two.

In figure 6 (a),  $\Delta S(T)$  for bifurcation from  $\alpha_+$  at  $T = 16.878$  is plotted. Though bifurcation is both sides, the bifurcating solution also bifurcate soon at  $T = 16.875$ . Thus there exist two bifurcated solutions for  $T > 16.875$ . For  $16.875 < T < 16.878$

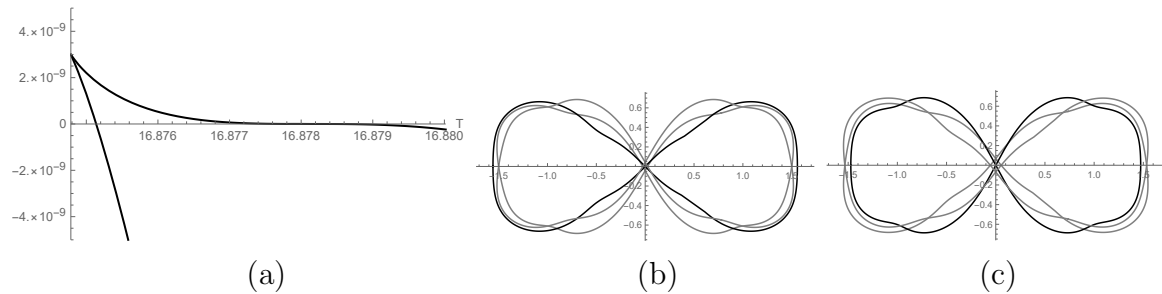


**Figure 6.** Bifurcation of  $\alpha_+$  at  $T = 16.878$  yielding  $D_{xy}$  solutions. (a)  $\Delta S(T)$ , (b)  $D_{xy}$  for  $T = 20$  from the right side of bifurcation point, and (c) from the left side. Parameters  $(x, y, v; d)$ : (b)  $(0.77903, 0.54721, 0.59844; -0.042907)$ , (c)  $(0.73650, 0.54718, 0.59824; 0.068048)$ .

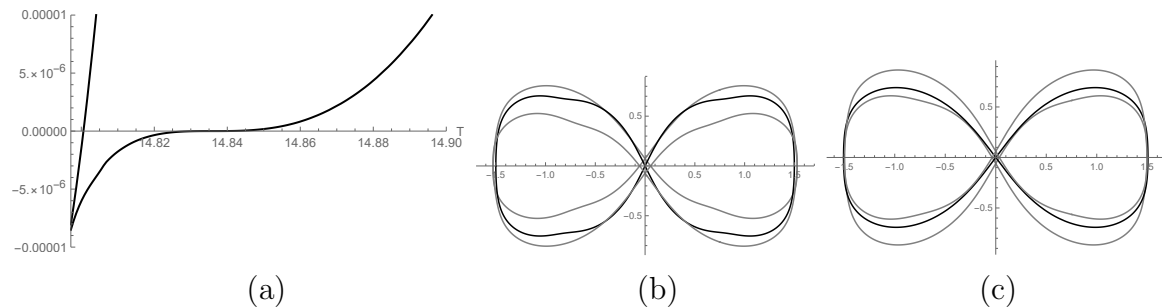


**Figure 7.** Bifurcation of  $\alpha_-$  at  $T = 14.836$  yielding  $D_{xy}$  solutions. (a)  $\Delta S(T)$ , (b)  $D_{xy}$  for  $T = 20$  from the right side of bifurcation point, and (c) from the left side. Parameters  $(x, y, v; d)$ : (b)  $(0.74968, 0.76413, 0.45966; 0.072840)$ , (c)  $(0.75349, 0.56442, 0.64295; -0.059918)$ .

both solutions are bifurcated from left side of bifurcation point but for  $T > 16.878$  one from right side and the other from left side. In figure 6 (b) and (c), the two bifurcated solutions for  $T = 20$  from both sides are shown with parameters  $(x, y, v)$  and  $d$ . In figure 7, bifurcation of  $D_{xy}$  solution from  $\alpha_-$  at  $T = 14.836$  is shown as figure 6 for  $\alpha_+$ .

The points indicated by  $D$  in table 2,  $T = 16.111$  for  $\alpha_+$  and  $T = 14.861$  for  $\alpha_-$ , yield  $D_x$  and  $D_2$  solutions represented by (51) and (52), respectively, as in the section 3.2. The bifurcations are one side in the right side and the number of incongruent bifurcating solutions  $N_B$ 's are both two. In figures 8 and 9,  $\Delta S(T)$  and the bifurcated solutions for  $T = 20$  are shown with parameters.

#### 4.2. Choreographic bifurcation

The points with  $|\Delta N| = 1$  in table 2,  $T = 18.615$  and  $T = 17.132$  for  $\alpha_+$ , and  $T = 14.595$  for  $\alpha_-$ , bifurcate choreographic solutions since the varied orbit  $Q$  for  $g = |\Delta N| = 1$ ,

$$Q = q + h\psi^{(1)}, \quad (55)$$

is choreographic,  $\hat{C}Q = Q$  [8, 20].

At  $T = 14.595$  for  $\alpha_-$ , the varied orbit  $Q$  is symmetric in the  $x$  axis as shown in figure 10 (a). We denote this orbit by  $C_x$ . Conditions for  $q(t)$  to be  $C_x$ , derived

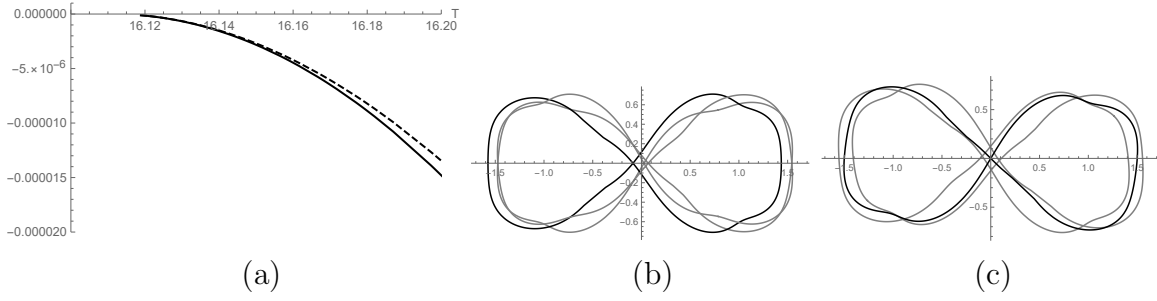


**Figure 8.** Bifurcation of  $\alpha_+$  at  $T = 16.111$  yielding  $D_x$  and  $D_2$  solutions. (a)  $\Delta S(T)$  for  $D_x$  solution (full curve) and for  $D_2$  (dashed curve). (b)  $D_x$  solution and (c)  $D_2$  for  $T = 20$ .  $D_2$  is rotated by  $\theta_2$  in (53). Parameters; (b)  $(x, y, v, l) = (0.78752, 0.54620, 0.59854, 0.0028781)$ , (c)  $(x, u, v; \Delta I) = (1.3362, 0.16921, 0.34182, 1.3573)$ .

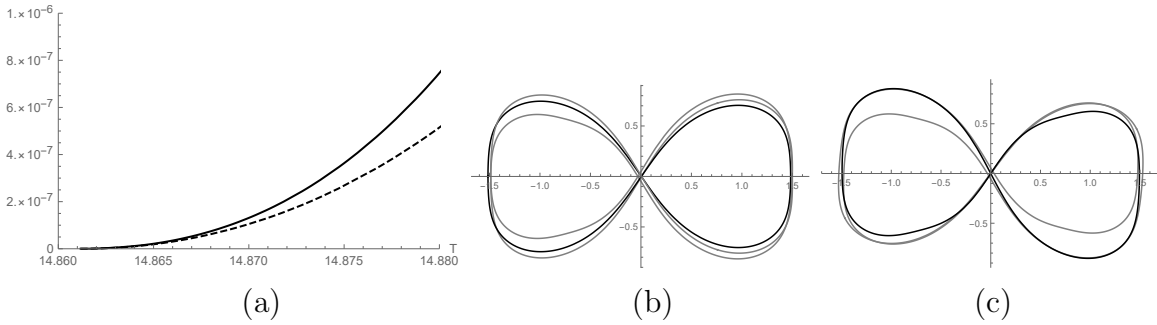


**Figure 9.** Bifurcation from  $\alpha_-$  at  $T = 14.861$  yielding  $D_x$  and  $D_2$  solutions. (a)  $\Delta S(T)$  for  $D_x$  solution (full curve) and for  $D_2$  (dashed curve). (b)  $D_x$  solution and (c)  $D_2$  for  $T = 20$ .  $D_2$  is rotated by  $\theta_2$  in (53). Parameters; (b)  $(x, y, v, l) = (0.75744, 0.72602, 0.52093, 0.027042)$ , (c)  $(x, u, v; \Delta I) = (1.5333, 0.061120, 0.33256; -0.52266)$

in Appendix A.3, are that  $q(t)$  takes an isosceles triangle configuration shown by filled circles in figure 10 (a), (36) and (37) with (44) at  $t = 0$  by parameters  $(x, y, v, l)$ , and opposite isosceles triangle configuration at  $t = T/6$  shown by open circles in figure 10 (a),

$$(q_6, \dot{q}_5, q_1 - q_3, \dot{q}_2 - \dot{q}_4) = 0. \quad (56)$$

For given period  $T$ , four conditions (56) determine four parameters  $(x, y, v, l)$ . An index to distinguish solution  $C_x$  from figure-eight choreography is  $l \neq 0$ . In figure 11 (a), the orbit of the solution  $C_x$  for  $T = 20$  bifurcated at  $T = 14.595$  from  $\alpha_-$  is shown with parameters  $(x, y, v, l)$ .

At  $T = 18.615$  for  $\alpha_+$ , the variated orbit  $Q$  is symmetric at origin as shown in figure 10 (b). We denote this orbit by  $C_2$ . Conditions for  $q(t)$  to be  $C_2$ , derived in Appendix A.5, are that  $q(t)$  takes an Euler configuration shown by filled circles in figure 10 (b), (47) and (48) at  $t = 0$  by parameters  $(x, u, v)$ , and another Euler configuration at  $t = T/6$  shown by open circles in figure 10 (b),

$$(q_1, q_2, \dot{q}_1 \dot{q}_6 - \dot{q}_2 \dot{q}_5) = 0. \quad (57)$$

For given period  $T$ , three conditions (57) determine three parameters  $(x, u, v)$ . An index

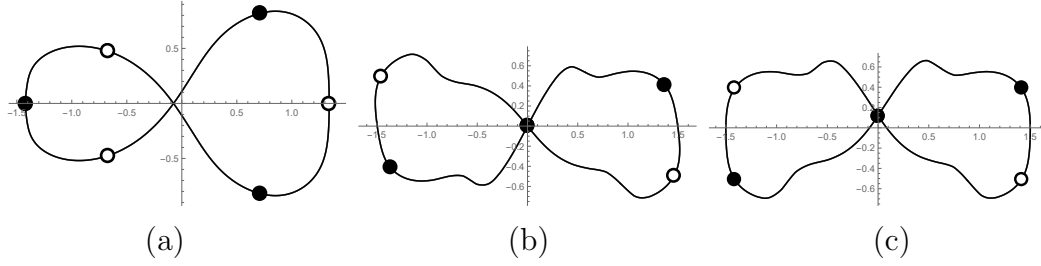


**Figure 10.** Varied orbit  $Q$  for LJ  $\alpha$  solution. (a)  $C_x$  in  $\alpha_-$ ;  $T = 15.215$ ,  $h = 1.5$  and  $\lambda = 0.43026$ . Filled circles are isosceles triangle configuration at  $t = 0$  and open circles at  $t = T/6$ . (b)  $C_2$  in  $\alpha_+$ ;  $T = 18.337$ ,  $h = 0.8$  and  $\lambda = 0.0027783$ . Filled circles are Euler configurations at  $t = 0$  and open circles at  $t = T/6$ . (c)  $C_y$  in  $\alpha_+$ ;  $T = 18.337$ ,  $h = 0.8$  and  $\lambda = -0.023907$ . Filled circles are configuration where a body on the  $y$  axis at  $t = 0$  and open circles at  $t = T/6$ .

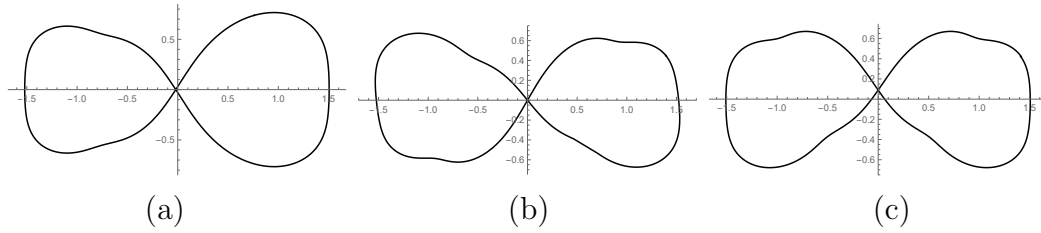


**Figure 11.** Choreographic solutions for  $T = 20$ ; (a)  $C_x$  bifurcating from  $\alpha_-$  at  $T = 14.595$ , (b)  $C_2$  from  $\alpha_+$  at  $T = 18.615$ , (c)  $C_y$  from  $\alpha_+$  at  $T = 17.132$ .  $C_2$  is rotated by  $\theta_2$  in (53). Parameters; (a)  $(x, y, v, l) = (0.76038, 0.73802, 0.49633, 0.096581)$ , (b)  $(x, u, v, \Delta I) = (1.4638, 0.11916, 0.30699, 0.48813)$ , (c)  $(x, y, u, v, w, y') = (1.4167, 0.42115, -0.19613, 0.27560, -0.52564, 0.089593)$ .

to distinguish solution  $C_2$  from figure-eight choreography is  $\Delta I \neq 0$ . In figure 11 (b), the orbit of the solution  $C_2$  for  $T = 20$  bifurcated at  $T = 18.615$  from  $\alpha_+$  is shown with parameters  $(x, y, v)$  and  $\Delta I$ .

At  $T = 17.132$  for  $\alpha_+$ , the varied orbit  $Q$  is symmetric in the  $y$  axis as shown in figure 10 (c). We denote this orbit by  $C_y$ . Conditions for  $q(t)$  to be  $C_y$ , derived in Appendix A.6, are that a body is on the  $y$  axis at  $t = 0$  shown by filled circles in figure 10 (c),

$$q(0) = (x, y, -x, -y - y', 0, y'), \quad (58)$$

$$\dot{q}(0) = (u, v, -u - s, -v - w, s, w), \quad (59)$$

where

$$s = \frac{2(xv - yu) + xw - y'u}{2y' + y} \quad (60)$$

by parameters  $(x, y, u, v, w, y')$ , and its inversion in the  $y$  axis at  $t = T/6$  shown by open circles in figure 10 (c),

$$(q_1, q_3 + x, q_4 - y, \dot{q}_4 + u, \dot{q}_5 - v, q_2 - y') = 0. \quad (61)$$

For given period  $T$ , the six conditions (61) determine six parameters  $(x, y, u, v, w, y')$ . An index to distinguish solution  $C_y$  from figure-eight choreography is  $y' \neq 0$ . In figure 11 (c),

the orbit of the solution  $C_y$  for  $T = 20$  bifurcating at  $T = 17.132$  from  $\alpha_+$  is shown with  $(x, y, u, v, w, y')$ .

For these three choreographies  $C = C_x, C_2, C_y$ , the variated orbit  $Q$  in (55) is written as

$$Q^C = q \pm h\psi^{(1)}. \quad (62)$$

The sign in front of  $h$  effects inversion of the orbit in the  $y$  axis for  $C_x$ , and in the  $x$  axis for  $C_2$  and  $C_y$ . These couples of congruent orbits bifurcate in the right side of the bifurcation point and  $N_B = 1$ .

## 5. Summary and discussions

In this paper, we showed that the Morse index changes at a bifurcation point for periodic solution and inversely all points where the Morse index changes are bifurcation points for figure-eight choreography under homogeneous potential with  $a \geq 0$  and for the  $\alpha$  solutions under LJ-type potential. Thus, for these choreographies, change of the Morse index,  $\Delta N \neq 0$ , is not only necessary but also sufficient condition for bifurcation point. Further we observed that  $\Delta N$  determines the number of incongruent bifurcating solutions  $N_B$  as (32).

The bifurcations are confirmed numerically by Newton's method. If the number of parameters is three as in the  $D_{xy}$ ,  $D_2$  and  $C_2$  cases, the parameters of the solution are represented graphically like [6]. At  $t$  satisfying one of the three conditions under some restriction  $f = \text{const}$  where  $f$  is a function of the three parameters, the rest conditions are given by two curves in the plane of two parameters. In figure 12, for solution  $D_{xy}$  determined by three parameters  $(x, y, v)$  in  $a = 1$  homogeneous system, at  $t$  satisfying  $q_4(t) = 0$ , the two conditions  $q_2(t) = 0$  and  $\dot{q}_1(t)\dot{q}_6(t) - \dot{q}_2(t)\dot{q}_5(t) = 0$  are shown in  $(x, y)$  plane with total energy

$$E = \frac{1}{2} \sum_{i=1}^6 \dot{q}_i^2 + U(q) \quad (63)$$

as a restriction. The parameter  $(x, y)$  for the  $D_{xy}$  solution and the figure-eight choreography are observed as crossing points of two curves in figure 12.

Newton's method sometimes does not converge unless initial parameters are good enough. We introduced another graphically assisted method: draw one condition as a function of one parameter by Newton's method in one lower dimension. In figure 13, for solution  $D_x$  determined by four parameters  $(x, y, v, l)$  in  $a = 1.3425$  homogeneous system,  $\dot{q}_3$  in (45) are shown as a function of  $v$  which is obtained by 4 - 1 dimensional Newton's method for the rest of three parameters  $(x, y, l)$  with the rest of three conditions  $(q_4, q_1 - q_5, \dot{q}_2 - \dot{q}_6) = 0$ . Zero about  $v = 2.5$  corresponds to figure-eight choreography and two other zeros  $D_x$  solutions in figure 13.

It is useful to evaluate the Euler characteristics

$$\chi = \sum_{q'} (-1)^{N(q')} \quad (64)$$

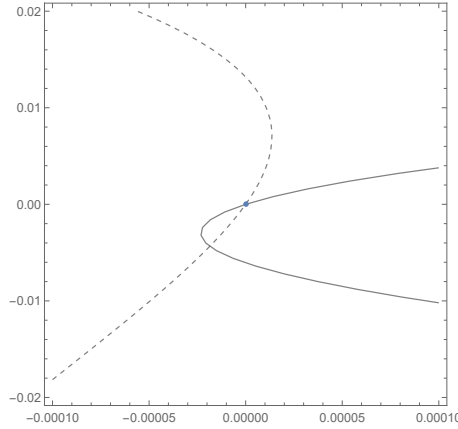


**Figure 12.** Map to search  $D_{xy}$  solution. Full and dashed curves are  $q_2(t) = 0$  and  $\dot{q}_1(t)\dot{q}_6(t) - \dot{q}_2(t)\dot{q}_5(t) = 0$ , respectively, at  $t$  satisfying  $q_4(t) = 0$  for  $q(t)$  starting from the initial conditions (36)–(38) with  $E = -0.69571$  for  $a = 1$  homogeneous potential. Horizontal and vertical axes are  $x - x_0$  and  $y - y_0$ , respectively, where  $(x_0, y_0)$  is  $(x, y)$  for figure-eight choreography with  $T = 1$ . Crossing points of two curves show the parameters for the  $D_{xy}$  solutions and for the figure-eight choreography.

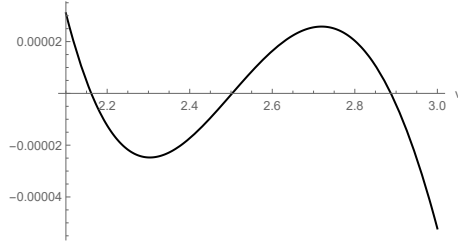


**Figure 13.**  $\dot{q}_3$  in (45) as a function of  $v$ . zero about  $v = 2.5$  corresponds to figure-eight choreography and two other zeros bifurcating solution  $D_x$ .

for the manifold of action functional in the domain of periodic functions, where  $N(q')$  is the Morse index at a periodic solution  $q'$ . Since the  $\chi$  will conserve, sometimes comparison of  $\chi$  at the both sides of the bifurcation point helps to find bifurcating solution.

We assume the Euler characteristics conserves at the both sides of bifurcation point, and (32) holds. Then we denote a number of congruent solutions which belong to the  $i$ th incongruent class by  $n_i$ , and their Morse index by  $N_i$ ,  $i = 1, 2, \dots, N_B$ .

For a bifurcation point with  $|\Delta N| = 1$ , bifurcation is one side since  $N_B = 1$ . From the conservation of  $\chi$  at the both sides of bifurcation point,

$$(-1)^N = (-1)^{N\pm 1} + n_1(-1)^{N_1} \quad (65)$$

we obtain  $n_1 = 2$  and  $(-1)^{N_1} = (-1)^N$ .

For a bifurcation point with  $|\Delta N| = 2$ , bifurcation can be one side or both sides since  $N_B = 2$ . For one side bifurcation, conservation of  $\chi$ ,

$$(-1)^N = (-1)^{N\pm 2} + n_1(-1)^{N_1} + n_2(-1)^{N_2} \quad (66)$$



**Table 3.** Restrictions of bifurcation by conservation of the Euler characteristics and (32). Symbols  $n_i$  and  $N_i$  are a number of congruent solutions which belongs to the  $i$ th incongruent class, and their Morse index, respectively,  $i = 1, \dots, N_B$ ,  $N_B = |\Delta N|$ .

$ \Delta N $	Bifurcation	Restriction for $n_i$	Restriction for $N_i$
1	one side	$n_1 = 2$	$(-1)^{N_1} = (-1)^N$
2	one side	$n_1 = n_2$	$(-1)^{N_1} = -(-1)^{N_2}$
2	both sides	$n_1 = n_2$	$(-1)^{N_1} = (-1)^{N_2}$

leads  $n_1 = n_2$  and  $(-1)^{N_1} = -(-1)^{N_2}$ . For both sides bifurcation,

$$(-1)^N + n_1(-1)^{N_1} = (-1)^{N \pm 2} + n_2(-1)^{N_2} \quad (67)$$

leads  $n_1 = n_2$  and  $(-1)^{N_1} = (-1)^{N_2}$ . In table 3, these restrictions on bifurcation are tabulated. According to the restriction for one side bifurcation at  $|\Delta N| = 2$  we found  $D_2$  solution after finding  $D_x$ .

The procedure to find bifurcation numerically by the Morse index is summarized as follows: 1) Find a point the Morse index changes,  $\Delta N \neq 0$ . 2) Investigate the corresponding variated orbit  $Q$  which is an approximation of bifurcating solution. Indeed, symmetry of  $Q$  is useful for numerical calculation. 3) If  $|\Delta N| > 1$ , variated orbit is chosen to make action critical. 4) Check conservation of the Euler characteristics at both sides of bifurcation point by table 3.

We leave the followings for future works: calculation of the Morse index for bifurcating solution; calculation of the Morse index for figure-eight choreography under homogeneous potential with negative  $a$ , that is,  $r^{-a}$  for  $a < 0$ ; tracking solutions bifurcated as much as possible; calculation of linear stability for figure-eight choreography and bifurcated solutions; conditions for the point the Morse index changes to be bifurcation point; and conditions for observation (32) on the number of bifurcating solutions to hold.

## Acknowledgments

We thank Kazuyuki Yagasaki for his valuable comment on variated orbits at Symposium on Celestial Mechanics and  $N$ -body Dynamics (2017). This work was supported by JSPS Grant-in-Aid for Scientific Research 17K05146 (HF) and 17K05588 (HO).

## Appendix A. Conditions for solutions

We derive conditions for  $q(t)$  to be  $D_{xy}$ ,  $D_x$ ,  $D_2$ ,  $C_x$ ,  $C_2$  and  $C_y$  solutions. We assume an inertia frame that total linear momentum  $P$  is zero,  $P = \sum_b \dot{\mathbf{r}}_b = 0$ , and center of mass  $G$  is at origin,  $G = \sum_b \mathbf{r}_b = 0$ . The subscript and index for body is assumed to be in the range 1 and 3.

For  $D_{xy}$ ,  $D_2$ ,  $C_2$  and  $C_y$ , total angular momentum  $l = \sum_b \mathbf{r}_b \times \dot{\mathbf{r}}_b$  is zero since sum of signed area of three orbits is zero from the symmetry of orbits.

A configuration that a body  $b$  is in the  $x$  axis and the other two bodies  $b \pm 1$  have the same  $x$  coordinate is called isosceles triangle configuration. For  $q(t)$  symmetric in the  $x$  axis conditions for isosceles triangle configuration is written as

$$(q_{2b}, \dot{q}_{2b-1}, q_{2b+1} - q_{2b-3}, \dot{q}_{2b+2} - \dot{q}_{2b-2}) = 0 \quad (\text{A.1})$$

by  $P = 0$ . For  $b = 2$  with  $x = q_1$ ,  $y = q_2$ ,  $v = \sqrt{\dot{q}_1^2 + \dot{q}_2^2}$  and total angular momentum  $l$ , (A.1) is written as (36), (37) and (44). The motion beginning from (A.1) is time reversal motion from (A.1) with inversion in the  $x$  axis and exchange of bodies  $b \pm 1$ .

A configuration that a body  $b$  is at origin is called as Euler configuration. For  $q(t)$  symmetric at origin a condition for Euler configuration is written as

$$(q_{2b-1}, q_{2b}, \dot{q}_{2b+1}\dot{q}_{2b-2} - \dot{q}_{2b+2}\dot{q}_{2b-3}) = 0 \quad (\text{A.2})$$

by  $G = 0$ . For  $b = 3$  with  $x = q_1$ ,  $u = \dot{q}_1$ ,  $v = \dot{q}_2$  (A.2) is written as (47) and (48). The motion beginning from (A.2) is time reversal motion from (A.2) with  $\pi$  rotation and exchange of bodies  $b \pm 1$ .

#### Appendix A.1. $D_{xy}$ solution

The  $D_{xy}$  solution takes initial conditions (36) and (37) with (38) and takes Euler configuration when body 2 reaches at origin at  $t = t'$ . Thus (A.2) with  $b = 2$ , (39) holds at  $t = t'$ . Thus at  $t = 2t'$ , three bodies take initial conditions with  $\pi$  rotation and exchange of bodies 1 and 3. Then at  $t = 4t'$ , three bodies take initial conditions again and the motion is periodic with period  $T = 4t'$ . Since the orbits were constructed by those from  $t = 0$  to  $t = T/2$  and their  $\pi$  rotation, the orbits are symmetric in the  $x$  and the  $y$  axes.

#### Appendix A.2. $D_x$ solution

The  $D_x$  solution takes initial conditions (36) and (37) with (38) and takes isosceles triangle configuration when body 2 reaches in the  $x$  axis again at  $t = t'$ . Then (A.1) with  $b = 2$ , (44) holds at  $t = t'$ . Then at  $t = 2t'$ , three bodies take initial conditions again and the motion is periodic with period  $T = 2t'$ . Since the orbits were constructed by those from  $t = 0$  to  $t = T/2$  and their inversion in the  $x$  axis, the orbits are symmetric in the  $x$  axis.

#### Appendix A.3. $C_x$ solution

The  $C_x$  solution takes initial conditions (36) and (37) with (38) and takes isosceles triangle configuration when body 3 reaches in the  $x$  axis again at  $t = t'$ . Then (A.1) with  $b = 3$ , (56) holds at  $t = t'$ . Then at  $t = 2t'$ , three bodies take initial conditions again but with cyclic permutation of bodies, and the motion is choreographic with period  $T = 3 \times 2t' = 6t'$ . Since the orbits were constructed by those from  $t = 0$  to  $t = T/6$  and their inversion in the  $x$  axis, the orbits are symmetric in the  $x$  axis.

*Appendix A.4.  $D_2$  solution*

The  $D_2$  solution takes initial conditions (47) and (48), and takes Euler configuration when body 2 reaches at origin at  $t = t'$ . Then (A.2) with  $b = 2$ , (49) holds at  $t = t'$ . Thus at  $t = 2t'$ , three bodies take initial conditions again and the motion is periodic with period  $T = 2t'$ . Since the orbits were constructed by those from  $t = 0$  to  $t = T/2$  and their  $\pi$  rotation, the orbits are symmetric at origin.

*Appendix A.5.  $C_2$  solution*

The  $C_2$  solution takes initial conditions (47) and (48), and Euler configuration when body 1 reaches in the  $x$  axis again at  $t = t'$ . Then (A.1) with  $b = 1$ , (57) holds at  $t = t'$ . Thus at  $t = 2t'$ , three bodies take initial conditions again with cyclic permutation of bodies, and the motion is choreographic with period  $T = 3 \times 2t' = 6t'$ . Since the orbits were constructed by those from  $t = 0$  to  $t = T/6$  and their  $\pi$  rotation, the orbits are symmetric at origin.

*Appendix A.6.  $C_y$  solution*

The  $C_y$  solution takes initial conditions (58) and (59) by  $G = P = 0$  with (60) by  $l = 0$  where body 3 is on the  $y$  axis, which are represented by six parameters. At  $t = t'$  when body 1 reaches in the  $y$  axis, the relation between the positions and velocities at  $t = t'$  have to be inversion in the  $y$  axis with exchange of bodies 2 and 3. Thus we have twelve relations but six conservation quantities,  $G$ ,  $P$ ,  $l$  and total energy, reduce it to six as (61). Thus at  $t = 2t'$  if (61) is satisfied, three bodies take initial conditions again with cyclic permutation of bodies, and the motion is choreographic with period  $T = 3 \times 2t' = 6t'$ . Since the orbits were constructed by those from  $t = 0$  to  $t = T/6$  and their inversion in the  $y$  axis, the orbits are symmetric in the  $y$  axis.

**References**

- [1] Moore C 1993 Braids in Classical Gravity *Phys. Rev. Lett.* **70** 3675–3679
- [2] Chenciner A and Montgomery R 2000 A remarkable periodic solution of the three-body problem in the case of equal masses *Annals of Mathematics* **152** 881–901
- [3] Simó C 2000 Dynamical properties of the figure eight solution of the three body problem *Contemporary Mathematics* **292** 209–228
- [4] Sbano L 2005 Symmetric solutions in molecular potentials *Proceedings of the international conference SPT2004, Symmetry and perturbation theory* (World Scientific Publishing, Singapore) 291–299
- [5] Sbano L and Southall J 2010 Periodic solutions of the N-body problem with Lennard-Jones-type potentials *Dynamical Systems* **25** 53–73
- [6] Fukuda H, Fujiwara T, Ozaki H 2017 Figure-eight choreographies of the equal mass three-body problem with Lennard-Jones-type potentials *J. Phys. A: Math. Theor.* **50** 105202
- [7] Shibayama M 2010 Numerical calculation of the second variation for the choreographic solution (in Japanese) *Proceedings of Symposium on Celestial Mechanics and N-body Dynamics 2010* ed. Saito M, Shibayama M and Sekiguchi M

- [8] Fukuda H, Fujiwara T, Ozaki H 2018 Morse index for figure-eight choreographies of the planar equal mass three-body problem *J. Phys. A: Math. Theor.* **51** 145201
- [9] Galán J, Muñoz-Almaraz F J, Freire E, Doedel E and Vanderbauwhede A 2002 Stability and Bifurcations of the Figure-8 Solution of the Three-Body Problem *Phys. Rev. Lett.* **88** 241101
- [10] Muñoz-Almaraz F J, Galán J and Freire E 2004 Families of symmetric periodic orbits in the three body problem and the figure eight *Monografías de la Real Academia de Ciencias de Zaragoza* **25** 229–240
- [11] Barutello V, Jadanza Riccardo D and Portaluri A 2016 Morse index and linear stability of the Lagrangian circular orbit in a three-body-type problem via index theory *A. Arch Rational Mech Anal* **219** 387
- [12] Hu X and Sun S 2010 Morse index and stability of elliptic Lagrangian solutions in the planar three-body problem *Advances in Mathematics* **223** 98–119
- [13] Hu X and Sun S 2009 Index and Stability of Symmetric Periodic Orbits in Hamiltonian Systems with Application to Figure-Eight Orbit *Commun. Math. Phys.* **290** 737
- [14] Muñoz-Almaraz F J and Vanderbauwhede A 2005 private communication
- [15] Muñoz-Almaraz F J, Galán J, Freire E and Vanderbauwhede A 2018 Numerical explorations in a modified potential of the TBP (Version v1.0) Zenodo. <http://doi.org/10.5281/zenodo.1500051>
- [16] Doedel E, Keller B H and Kernevez J P 1991 Numerical analysis and control of bifurcation problems (I): bifurcation in finite dimensions *International Journal of Bifurcation and Chaos* **1** No. 3 493–520
- [17] Doedel E, Keller B H and Kernevez J P 1991 Numerical analysis and control of bifurcation problems (II): bifurcation in infinite dimensions *International Journal of Bifurcation and Chaos* **1** No. 4 745–772
- [18] Chenciner A 2003 Some facts and more questions about the Eight *Topological Methods, Variational Methods and Their Applications, Proceedings of the ICM 2002 Satellite Conference on Nonlinear Functional Analysis* (World Scientific) 77–88
- [19] Shibayama M 2018 private communication
- [20] Fujiwara T, Fukuda H and Ozaki H 2018 Decomposition of the Hessian matrix for action at choreographic three-body solutions with figure-eight symmetry arXiv:1811.09023